nature climate change

ARTICLES

https://doi.org/10.1038/s41558-018-0350-3

Natural variability of Southern Ocean convection as a driver of observed climate trends

Liping Zhang[1,2*], Thomas L. Delworth[1,2], William Cooke[2,3] and Xiaosong Yang[2,3]

Observed Southern Ocean surface cooling and sea-ice expansion over the past several decades are inconsistent with many historical simulations from climate models. Here we show that natural multidecadal variability involving Southern Ocean convection may have contributed strongly to the observed temperature and sea-ice trends. These observed trends are consistent with a particular phase of natural variability of the Southern Ocean as derived from climate model simulations. Ensembles of simulations are conducted starting from differing phases of this variability. The observed spatial pattern of trends is reproduced in simulations that start from an active phase of Southern Ocean convection. Simulations starting from a neutral phase do not reproduce the observed changes, similarly to the multimodel mean results of CMIP5 models. The long timescales associated with this natural variability show potential for skilful decadal prediction.

While Arctic sea ice is rapidly decreasing in association with increasing surface air temperature[1], observations clearly show an expansion of Southern Ocean (SO) sea-ice extent (SIE)[2] during the satellite era (1979–2012) (Fig. 1a). This modest increase is consistent with the observed SO cooling trend (Fig. 1a). The sea surface temperature (SST) and sea-ice concentration (SIC) trends are not homogeneous in space[3,4], with opposing signs in the Amundsen-Bellingshausen seas versus the Ross and Weddell seas (Fig. 1b,c). Several mechanisms have been proposed to explain these trends[3–16]. A leading idea involves surface wind changes[3–14] driven by a number of factors, including a positive trend of the Southern Annular Mode in response to stratospheric ozone depletion, or a deepened Amundsen Sea Low driven by remote tropical Pacific or North Atlantic SST anomalies. In these studies, the wind-driven surface heat flux, upper ocean dynamics and sea-ice drift are key drivers for the observed sea-ice and SST dipoles. Another explanation involves surface freshening[15,16] caused by anthropogenic warming, possibly via global water cycle amplification and/or the melting of Antarctic glaciers and ice sheets. The surface freshening enhances stratification and suppresses convective mixing with the warmer water at depth, producing cold SST anomalies and thus inhibiting the melting of Antarctic sea ice. However, other studies argue that wind anomalies, induced by ozone depletion, favour an overall decrease rather than increase of Antarctic sea ice[17], and that the surface freshening caused by anthropogenic warming is not large enough to trigger sea-ice expansion[18,19].

In this study we examine the possibility that internal variability involving deep ocean convection in the SO could be a major contributor to the observed trends, probably in concert with other previously identified factors. To explore this, we use simulations with a newly developed coupled ocean–atmosphere sea-ice model (SPEAR_AM2—see Methods for model details). When this model is driven with estimates of changes in past radiative forcing, the model simulation does not reproduce the observed SST and SIC trends around the Antarctic. Instead, the model simulates a steady warming and Antarctic sea-ice loss (Fig. 1d,e), as is commonly seen in multimodel mean results of Coupled Model Intercomparison Project Phase 5 (CMIP5) models[20]. One possible explanation for the discrepancy between observations and model projections is that natural variability may play a large role in the observed trends[21,22]. Indeed, the observed sea-ice expansion is within the range of natural variability in the control run[2,21,22].

We provide additional evidence supporting a strong role for natural variability in the observed trends, probably involving multidecadal modulation of SO convection and deep-water formation. As shown below, various aspects of the observed changes are consistent with a multidecadal weakening of Antarctic bottom water (AABW) formation. In the 1970s, the open ocean Weddell Polynya[23,24] (Supplementary Fig. 1) was first seen by satellite. After 1976, no similar Weddell Polynya was observed until 2016. Ship-based hydrographic observations show that the AABW has warmed globally between the 1980s and 2000s[25,26]. Objectively analysed ocean data also exhibit a warming temperature trend in the SO subsurface and a cooling trend in the surface (Supplementary Fig. 2). Both warming trends are consistent with weakened convection. These observational results suggest a global-scale slowdown of the bottom, southern limb of the meridional overturning circulation (MOC) during 1979–2012[25]. Meanwhile, multidecadal variability of SO SST[27,28] shown in reanalysis (Fig. 1a) and palaeoclimate records[29,30] highlights the low-frequency character of SO climate and places the recent Antarctic sea-ice trends into a broader context.

SO internal variability in coupled model

In order to compare the observed changes with an estimate of natural variability, we first examine SO natural climate variability from an extended simulation of the SPEAR_AM2 model. We see that the time series of the AABW cell, related to ocean convection (Methods and Supplementary Figs. 3–5), has pronounced multidecadal to centennial-scale fluctuations that begin after an initial 1,000 year spin-up (Fig. 2a). When convection is strong, the mixed layer depth (MLD) is largest in the open Weddell Sea, near the Maud Rise (65° S, 0°) (Fig. 2b). This convection location resembles the observed 1974–1976 Weddell Polynya (Supplementary Fig. 1). Some MLD changes are also seen over the Antarctic continental shelves, such as in the west Ross, Weddell seas and East Antarctic, but the magnitude is much smaller than that in the open ocean

[1]Atmospheric and Oceanic Science, Princeton University, Princeton, NJ, USA. [2]NOAA/Geophysical Fluid Dynamics Laboratory, Princeton, NJ, USA. [3]University Corporation for Atmospheric Research, Boulder, CO, USA. *e-mail: Liping.Zhang@noaa.gov

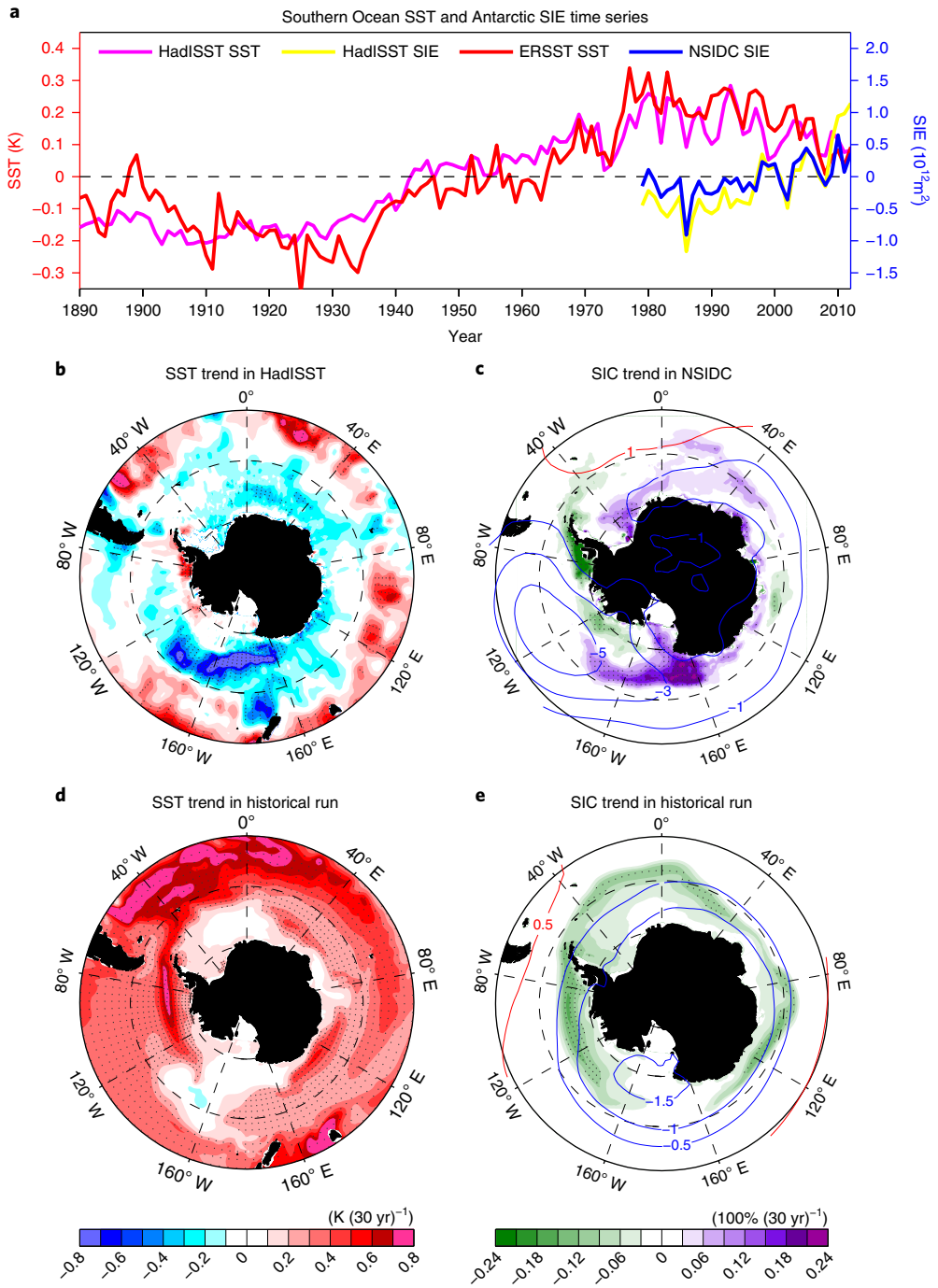

Fig. 1 | Annual SST and sea-ice time series and trends. a, Time series of SO area mean (50°–70°S) SST (K) anomalies over 1890–2012 and SIE (10^{12} m^2) anomalies over 1979–2012. These anomalies are with respect to their long-term mean values. The SST data are from Hadley Centre Sea Ice and Sea Surface Temperature (HadISST) and Extended Reconstructed Sea Surface Temperature (ERSST) version 3. The sea-ice data are from HadISST and the National Snow and Ice Data Center (NSIDC). **b**, SST trend in HadISST over 1979–2012. **c**, SIC and SLP trends in NSIDC over 1979–2012. **d**,**e**, SST (**d**) and SIC/SLP (**e**) trends in ensemble mean results of SPEAR_AM2 historical run over 1979–2012. Units are K(30 yr)$^{-1}$ for the SST trend, 100%(30 yr)$^{-1}$ for the SIC trend and hPa(30 yr)$^{-1}$ for the SLP trend. Stippling on trends means that the trend is significant at the 95% level based on a two-sided Student *t*-test. Note that the trend pattern is not sensitive to the choice of ending year from 2010 to 2015 (Methods).

(Fig. 2b). The internal low-frequency variability over the SO is also found in other models[31–37]. The physical mechanisms behind such multidecadal fluctuations have much in common with similar variability found in the Kiel Climate Model[35] and the GFDL CM2.1 model[36,37] (Supplementary Figs. 6 and 7). Briefly, the occurrence of deep convection is caused by the build-up of heat in the subsurface ocean, where the heat originates from the transport of relatively warm water from the north by the subpolar gyre. The heat build-up in the subsurface eventually destabilizes the water column, leading to deep convection and large heat release from the subsurface ocean. The depletion of the subsurface heat reservoir, combined with surface freshening primarily due to sea-ice melting, creates a

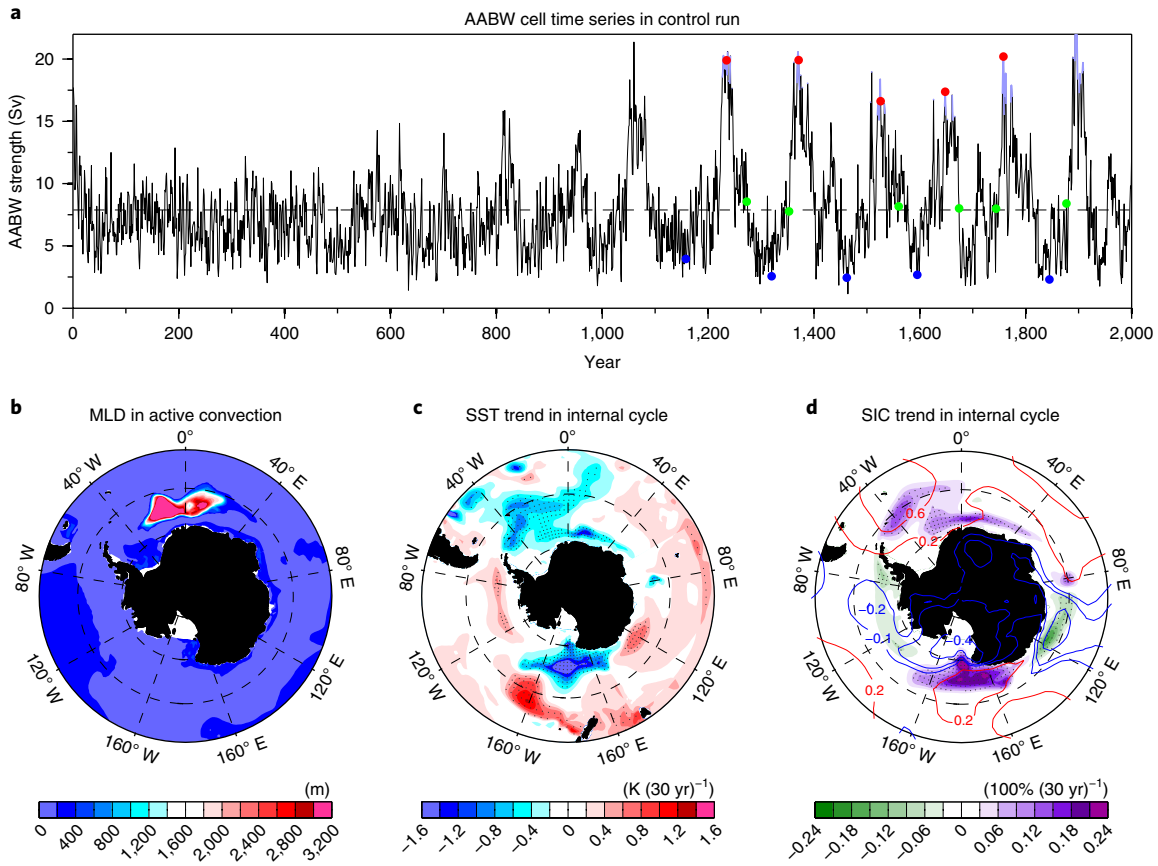

Fig. 2 | SO internal variability in the pre-industrial control run. Analyses of output from a pre-industrial control simulation. **a**, Time series of the annual mean AABW cell index in a control run. The AABW index is defined each year as the absolute value of the minimum in the global overturning stream function in density space south of 60° S. Red (blue, green) dots show the periods used to initialize additional simulations (described in text) that are characterized by strong (weak, average) convective activity in the SO. The purple line overlying the AABW cell index time series denotes years when the Weddell Polynya appears in September, October or November. **b**, Composite of September MLD for active convection (red dots in **a**). **c**,**d**, Map of trends in annual mean SST (K(30 yr)$^{-1}$) (**c**) and SIC (100%(30 yr)$^{-1}$) and SLP (hPa(30 yr)$^{-1}$) (**d**) for the 30 years following a maximum in convective activity. Stippling on trend maps indicates that the trend is significant at the 95% level based on a two-sided Student *t*-test. For the trend patterns, data are 30 yr low-pass filtered before composite analysis.

strong vertical stratification leading to greatly reduced convection. The multidecadal timescale of SO convection is primarily determined by the rate of subsurface warming and surface freshening. In addition, the deep convection initiates a positive sea ice–ocean feedback[38] in the upper Ross Sea (Supplementary Fig. 8). The brine released as a result of ice formation is transported to deeper layers, leading to a strong stratification, a shallower mixed layer, and thus reduced movement of heat from the subsurface to the surface. This leads to surface cooling and an increase of sea ice, forming a positive ice-coverage–heat-storage feedback.

Using composite analyses during a convective cycle in the model, we show that this natural variability can produce approximately 30 yr trends in SST and SIC (Fig. 2c,d) that resemble the observations, with cooling trends in the Ross and Weddell seas and warming trends over the Amundsen–Bellingshausen seas (Fig. 2c versus Fig. 1b). Although there are differences in amplitude (modelled amplitude is almost twice that of observations, which may be due to different sensitivities in model and observations), the spatial correlation between the modelled and observed SST trends is 0.65. The SIC trend also broadly agrees with observations, in both spatial pattern and magnitude (Fig. 2d versus Fig. 1c). In contrast, the sea-level pressure (SLP) trend shows a large discrepancy between the internal cycle and observations, in which the observed SLP trend is one order of magnitude larger than that modelled (Fig. 2d versus Fig. 1c). The observed wind trend in the SO is largely associated with anthropogenic forcings[39] and remote tropical SST anomalies[10–12], while the SLP trend in the internal cycle primarily reflects the middle- and high-latitudinal ocean feedback to the atmosphere, which is much smaller than the atmosphere forcing (Supplementary Figs. 9 and 10). This large wind difference also provides evidence that the SO wind may not be the only factor generating the observed SST/SIC trend patterns. A close inspection reveals that the phase lag of convection between the Weddell/Ross seas and Amundsen–Bellingshausen seas during the internal cycle determines the SST/SIC pattern seen in Fig. 2c,d (Supplementary Figs. 11 and 12). After convection peaks, the weakening convection over the Weddell and Ross seas gradually suppresses convective mixing with warm subsurface water, in turn leading to the cooling surface and increasing sea ice. The Amundsen–Bellingshausen seas, however, respond slowly with several years' delay, due to the advection time of salinity anomalies from the Ross Sea (Supplementary Fig. 12c). Once subsurface heating initiates convection, salty water in the upper layer is advected over adjoining marginally stable water columns, and initiates convection in them. The convection over the Amundsen–Bellingshausen seas first strengthens due to delayed response, then gradually weakens following other basins. The overall 30 yr trend there eventually exhibits weak warming and decreasing sea ice.

Initial-condition dependence of transient climate response

The similarity between the SST/SIC trends in observations and those associated with internal variability in the control run suggests that natural internal variability associated with SO convection may play a significant role in the observed trends. We provide further support for this by conducting simulations that are forced by realistic time-evolving radiative forcing (Methods). We conduct three sets of simulations: the first set uses ocean initial conditions from an active convective phase of the variability, the second set uses ocean initial conditions from a neutral phase and the third uses ocean initial conditions from an inactive convective phase, as illustrated in Fig. 2a. The historical simulations initialized from an active state are intended to resemble the period in the 1970s with the Weddell Polynya, and presumably active convection over the SO.

When initialized from a strong convective phase of the natural variability, the simulated convection and AABW cell exhibits a decreasing trend over the course of the simulation from the 1970s through to 2012 (Fig. 3a). Remarkably, this simulation captures the principal features of the observed SST/SIC trends, including the overall cooling trend and sea-ice expansion, the maximum cooling trend (sea-ice increase) over the Ross Sea and a warming trend (sea-ice decrease) in the Amundsen–Bellingshausen seas (Fig. 3b–d). Moreover, the surface–subsurface temperature dipole south of 55° S with cooling in the surface and warming in the subsurface (Fig. 3d) is broadly in agreement with observations (Supplementary Fig. 2). Heat budget analysis reveals that the cooling SST trends over the Weddell and Ross seas are dominated by the declining vertical mixing term (Supplementary Fig. 13), consistent with the AABW cell change.

Further examination finds that the SLP trend is much larger than that in the internal cycle because of the anthropogenic forcings[39] (Fig. 3c versus Fig. 2d), although it is still weak when compared with reanalysis (Fig. 3c versus Fig. 1c). This is a common bias in most coupled climate models[20] or may be due to the absence of internal tropical teleconnection as a result of ensemble averaging. The stronger Amundsen Low induces a cyclonic circulation, heating the Antarctic Peninsula by warm-air advection. In addition, the associated negative wind stress curl spins up the local subpolar gyre, causes the relatively warm and salty deep water to upwell[40], enhances local convective mixing and therefore favours warm SST anomalies over the Amundsen–Bellingshausen seas. This is why the SST/SIC trend over the Amundsen–Bellingshausen seas in Fig. 3b,c is much larger than that in the internal cycle (Fig. 2c,d). These two processes are also reflected in the heat budget horizontal advection and vertical mixing terms (Supplementary Fig. 13).

In stark contrast, historical simulations that start from an either inactive or neutral phase of the oscillation in SO convection produce totally different responses. The AABW cell shows an upward trend when the model is initialized with inactive convection (Fig. 3e). Accordingly, the SO experiences broad SST warming and sea-ice reduction due to the combined effects of anthropogenic forcing and convective warming (Fig. 3e–g). The SO subsurface shows a cooling trend, consistent with the spin-up of the AABW cell (Fig. 3h). The SO response that is started from neutral convection has similar features to the ensemble mean results of the historical runs in SPEAR_AM2 (Fig. 3i–l versus Fig. 1d,e) and CMIP5 models[20]. This suggests that the response here (Fig. 3i–l) is primarily due to anthropogenic forcing. The distinct responses among these three groups of experiments indicate that the SO transient response to global climate change is very sensitive to the initial conditions of deep convection. This highlights the crucial role of SO natural variability in determining the detectability of transient climate response to global warming[41].

Seasonality of sea-ice trend

We also examine the seasonality of sea-ice trends (Supplementary Fig. 14). Our historical simulations that started with active convection reasonably capture the observed warm-season (DJFMAM) sea-ice trend (Supplementary Fig. 14a,c,e). The success of the simulation is primarily due to synchronizing the slowly evolving SO convection internal variability with the model. The model performance of sea ice in the cold season (JJASON) is not as good as that in the warm season (Supplementary Fig. 14b,d,f). Note that the observed sea-ice trend position in JJASON is far away from the coast, shedding light on the importance of surface wind, which can cause sea-ice drift[42]. Note also that the wind trend in our historical simulations is only half the magnitude of that in the reanalysis (Fig. 3c versus Fig. 1c). To evaluate the importance of wind trends to the JJASON sea-ice trend, we conduct two additional groups of experiments in which we assimilate observed SLP variations into the model. This assimilation constrains the time series of model winds to resemble the time series of observed winds, so that we can assess the impact of the observed winds on the SST and sea-ice trends. One group starts from an active convective phase, and the other starts from a neutral convective phase (Methods). The simulations initialized from an active convective phase produce a better cold-season sea-ice trend, especially over the Antarctic Peninsula region (Supplementary Fig. 15a,b), thereby emphasizing the importance of wind trends. In contrast, simulations started from a neutral convective phase produce an overall sea-ice retreat, despite the fact that realistic surface winds are imposed on the model via SLP assimilation (Supplementary Fig. 15c,d). A close inspection reveals that the warm SST and decreasing sea ice here are primarily associated with the spin-up of the AABW cell (Supplementary Fig. 15c). When compared with the weak persistence of neutral convection, the strong and long-lasting westerly wind anomalies become dominant over the SO. The wind mechanically induces upwelling and in turn spins up the entire MOC[43]. This process is also consistent with the second stage of the previous two timescale arguments[44], in which the equilibrium response of the SO to an increase in surface westerlies is associated with the upwelling of warm water below, and thus the SO experiences broad warming anomalies in the surface. These results further highlight the significant role of SO deep convection in modulating transient climate response to wind change.

Discussion and summary

In the present study, we investigated the potential physical drivers responsible for the observed SO SST and sea-ice trends in recent decades. This is a critical goal in climate science, especially with the importance of the SO for the uptake of heat and carbon from the atmosphere. Observations suggest a weakening of SO convection and deep-water formation between the 1980s and 2000s, coincident with the overall surface cooling trend and increasing sea ice. Here we find that these observed trends are consistent with a particular phase of natural multidecadal variability of SO deep convection as derived from climate model simulations. Ensembles of climate change simulations are conducted starting from different phases of this variability. Simulations that start from an active phase of SO convection, such as may have occurred in the 1970s, can reproduce the observed pattern of SST and sea-ice trends, particularly during the warm season (DJFMAM). We argue that natural multidecadal variability of SO deep convection could modulate the transient climate response to anthropogenic forcings, and that weakening of SO deep convection is a potential driver for observed SST and sea-ice trends over the SO. Our argument here shares some similarities with that in refs [28,45].

However, we cannot conclude that internally generated SO deep convection is the only driver, even in recent observations. The SO deep-convection change could work together with various other mechanisms identified in earlier studies[3–16], such as wind-driven ice transport and cold/warm-temperature advection, and anthropogenic surface freshening due to an amplified hydrological cycle and ice-sheet melting. As mentioned above, the surface wind

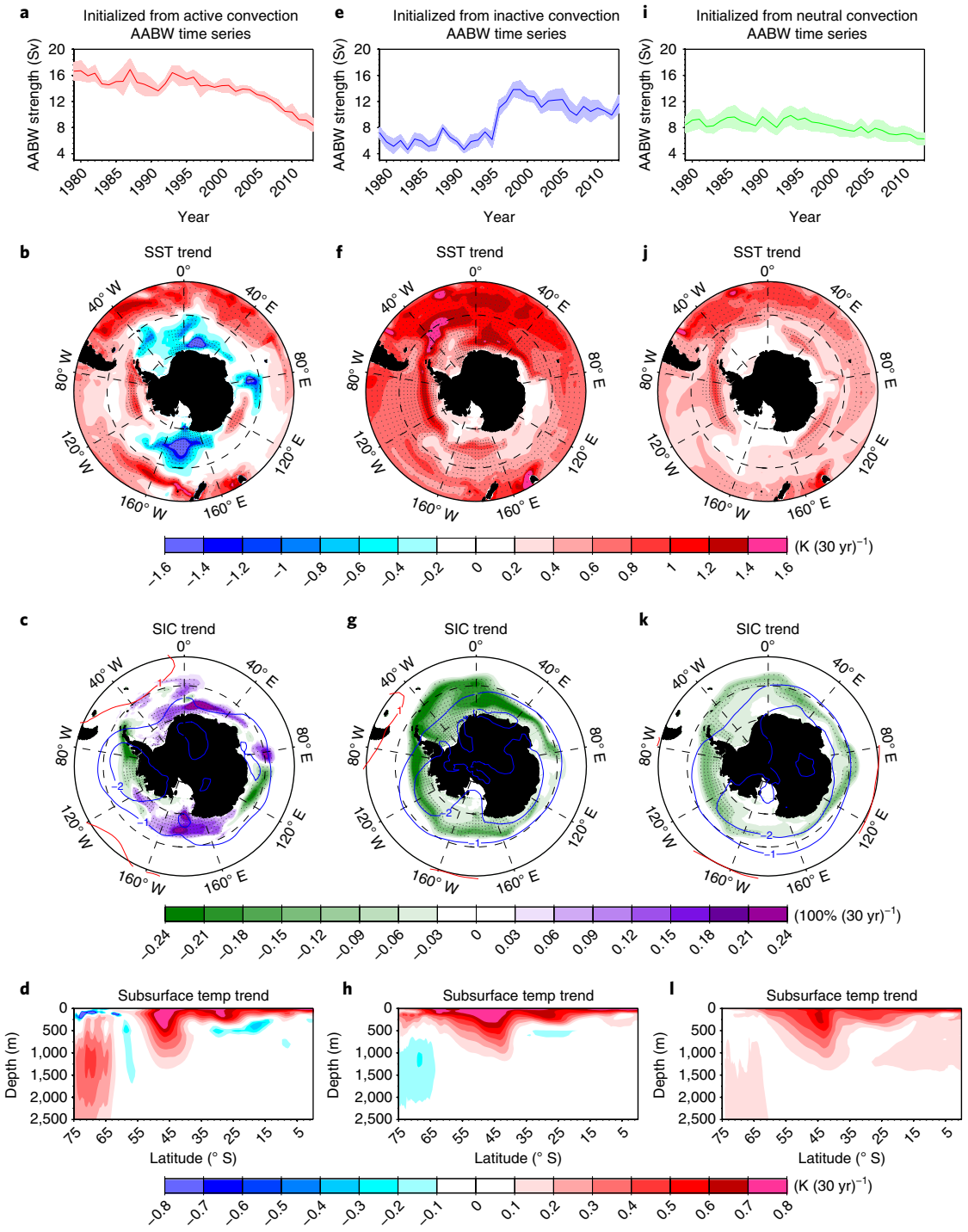

Fig. 3 | Dependence of transient climate response on the initial state of SO convection. a–d, The AABW cell time series (**a**), annual SST (**b**), SIC/SLP (**c**) and zonal mean subsurface temperature (**d**) trends over 1979–2012 in historical simulations initialized from a period with strong convection. **e–h**,**i–l**, The same as **a–d** but for simulations starting from states with weak and neutral convection, respectively. Units are Sv for the AABW cell, K(30 yr)$^{-1}$ for the SST and subsurface temperature trends, 100%(30 yr)$^{-1}$ for the SIC trend and hPa(30 yr)$^{-1}$ for the SLP trend. The shading in **a**,**e**,**i** denotes the ensemble spread (ensemble mean plus one standard deviation). Stippling on trends means that the trend is significant at the 95% level based on a two-sided Student *t*-test.

trend favours warm SST and decreasing sea ice over the Antarctic Peninsula through warm advection and over the Amundsen–Bellingshausen seas through enhanced vertical mixing caused by anomalous negative wind stress curl. Our model also shows that the long-lasting westerly winds over the SO induce upwelling and a spin-up of the AABW cell, which in turn generates the warm SST. The surface freshwater changes due to shifted storm tracks and melting ice sheet in future may slow down the SO MOC[15], which also cannot be excluded. It is also possible that melting of land-based ice sheets, a process usually not included in climate models, could cause surface freshening and the subsequent suppressed convection and SST cooling.

We need to consider all of the key factors and their interactions when interpreting the observations, including in detection and attribution studies. In reality, it is very likely that different processes dominate in different periods. The slowly weakening SO deep convection due to internal variability can be disrupted if the enhanced surface westerly winds and associated negative wind stress curl are persistent and strong enough. For example, the Weddell Polynya in 2016 is suggested to be caused by anomalously strong deepening of the Amundsen Sea Low[46] due to coincidence of strong negative Southern Annular Mode and La Niña-like SST anomalies in the tropics. The opposite is also possible when the internal variability overwhelms the wind effect.

In contrast to surface wind changes, variations of SO deep convection, whether from radiative forcing or internal variability, have very long timescales due to the large inertia of the subsurface ocean[36,47]. The persistence timescale of the natural variability of deep convection in the model used for this study is approximately 20 yr (Supplementary Fig. 16). To the extent that similar variability exists in the real climate system, this persistence makes the climate impacts associated with this variability potentially predictable, provided that we can properly initialize models using observational estimates of the three-dimensional state of the ocean. This calls for sustained in situ ocean observations in the SO, particularly in the subsurface ocean. Understanding the SO deep convection evolution will help us to better predict future changes in Antarctic sea ice and their far-reaching impacts on the global carbon cycle[48] and Antarctic marine ecosystems[49,50].

Online content

Any methods, additional references, Nature Research reporting summaries, source data, statements of data availability and associated accession codes are available at https://doi.org/10.1038/s41558-018-0350-3.

Received: 4 April 2018; Accepted: 30 October 2018;
Published online: 3 December 2018

References

1. Stroeve, J., Holland, M. M., Meir, W., Scambos, T. & Serreze, M. Arctic sea ice decline: faster than forecast. *Geophys. Res. Lett.* **34**, L09501 (2007).
2. Turner, J. et al. An initial assessment of Antarctic sea ice extent in the CMIP5 models. *J. Clim.* **26**, 1473–1484 (2013).
3. Stammerjohn, S., Martinson, D. G., Smith, R., Yuan, X. & Rind, D. Trends in Antarctic annual sea ice retreat and advance and their relation to El Niño-Southern Oscillation and Southern Annular Mode variability. *J. Geophys. Res.* **113**, C03S90 (2008).
4. Simpkins, G. R., Ciasto, L. M. & England, M. H. Observed variations in multidecadal Antarctic sea ice trends during 19792012. *Geophys. Res. Lett.* **40**, 3643–3648 (2013).
5. Holland, P. R. & Kwok, R. Wind-driven trends in Antarctic sea-ice drift. *Nat Geosci.* **5**, 872–875 (2012).
6. Kwok, R. & Comiso, J. C. Southern Ocean climate and sea ice anomalies associated with the Southern Oscillation. *J. Clim.* **15**, 487–501 (2002).
7. Turner, J. et al. Non-annular atmospheric circulation change induced by stratospheric ozone depletion and its role in the recent increase of Antarctic sea ice extent. *Geophys. Res. Lett.* **36**, L08502 (2009).
8. Matear, R. J., O'Kane, T. J., Risbey, J. S. & Chamberlain, M. Sources of heterogeneous variability and trends in Antarctic sea-ice. *Nat. Commun.* **6**, 8656 (2015).
9. Purich, A. et al. Tropical pacific SST drivers of recent Antarctic sea ice trends. *J. Clim.* **29**, 8931–8948 (2016).
10. Meehl, G. A., Arblaster, J. M., Bitz, C. M., Chung, C. T. Y. & Teng, H. Antarctic sea-ice expansion between 2000 and 2014 driven by tropical Pacific decadal climate variability. *Nat. Geosci.* **9**, 590–595 (2016).
11. Li, X., Holland, D. M., Gerber, E. P. & Yoo, C. Impacts of the north and tropical Atlantic Ocean on the Antarctic Peninsula and sea ice. *Nature* **505**, 538–542 (2014).
12. Ding, Q., Steig, E. J., Battisti, D. S. & Küttel, M. Winter warming in West Antarctica caused by central tropical Pacific warming. *Nat Geosci.* **4**, 398–403 (2011).
13. Lee, S.-K. et al. Wind-driven ocean dynamics impact on the contrasting sea-ice trends around West Antarctica. *J. Geophys. Res. Oceans* **122**, 4413–4430 (2017).
14. Zhang, L., Delworth, T. L. & Zeng, F. The impact of multidecadal Atlantic meridional overturning circulation variations on the Southern Ocean. Clim. Dynam. **48**, 2065–2085 (2017).
15. de Lavergne, C., Palter, J. B., Galbraith, E. D., Bernardello, R. & Marinova, I. Cessation of deep convection in the open Southern Ocean under anthropogenic climate change. *Nat. Clim. Change* **4**, 278–282 (2014).
16. Bintanja, R., Van Oldenborgh, G. J., Drijfhout, S. S., Wouters, B. & Katsman, C. A. Important role for ocean warming and increased ice-shelf melt in Antarctic sea-ice expansion. *Nat. Geosci.* **6**, 376–379 (2013).
17. Sigmond, M. & Fyfe, J. C. Has the ozone hole contributed to increased Antarctic sea ice extent? *Geophys. Res. Lett.* **37**, L18502 (2010).
18. Swart, N. C. & Fyfe, J. C. The influence of recent Antarctic ice sheet retreat on simulated sea ice area trends. *Geophys. Res. Lett.* **40**, 4328–4332 (2013).
19. Pauling, A. G., Bitz, C. M., Smith, I. J. & Langhorne, P. J. The response of the Southern Ocean and Antarctic sea ice to freshwater from ice shelves in an earth system model. *J. Clim.* **29**, 1655–1672 (2016).
20. Purich, A., Cai, W., England, M. H. & Cowan, T. Evidence for link between modelled trends in Antarctic sea ice and underestimated westerly wind changes. *Nat. Commun.* **7**, 10409 (2016).
21. Zunz, V., Goosse, H. & Massonnet, F. How does internal variability influence the ability of CMIP5 models to reproduce the recent trend in Southern Ocean sea ice extent? *Cryosphere* **7**, 451–468 (2013).
22. Polvani, L. M. & Smith, K. L. Can natural variability explain observed Antarctic sea ice trends? New modeling evidence from CMIP5. *Geophys. Res. Lett.* **40**, 3195–3199 (2013).
23. Martinson, D. G., Killworth, P. D. & Gordon, A. L. A convective model for the Weddell Polynya. *J. Phys. Oceanogr.* **11**, 466–488 (1981).
24. Gordon, A. L. Weddell deep water variability. *J. Mar. Res.* **40**, 199–217 (1982).
25. Purkey, S. G. & Johnson, G. C. Global contraction of Antarctic bottom water between the 1980s and 2000s. *J. Clim.* **25**, 5830–5844 (2012).
26. Purkey, S. G. & Johnson, G. C. Antarctic bottom water warming and freshening: contributions to sea level rise, ocean freshwater budgets, and global heat gain. *J. Clim.* **26**, 6105–6122 (2013).
27. Fan, T., Deser, C. & Schneider, D. P. Recent Antarctic sea ice trends in the context of Southern Ocean surface climate variations since 1950. *Geophys. Res. Lett.* **41**, 2419–2426 (2014).
28. Latif, M., Martin, T. & Park, W. Southern Ocean sector centennial climate variability and recent decadal trends. *J. Clim.* **26**, 7767–7782 (2013).
29. Cook, E. R., Buckley, B. M., D'Arrigo, R. D. & Peterson, M. J. 2000. Warm-season temperatures since 1600 BC reconstructed from Tasmanian tree rings and their relationship to large-scale sea surface temperature anomalies. *Clim. Dynam.* **16**, 79–91 (2000).
30. LeQuesne, C., Acuña, C., Boninsegna, J. A., Rivera, A. & Barichivich, J. Long-term glacier variations in the central Andes of Argentina and Chile, inferred from historical records and tree-ring reconstructed precipitation. *Palaeogeogr. Palaeoclimatol. Palaeoecol.* **281**, 334–344 (2009).
31. Zanowski, H., Hallberg, R. & Sarmiento, J. L. Abyssal ocean warming and salinification after Weddell polynyas in the GFDL CM2G coupled climate model. *J. Phys. Oceanogr.* **45**, 2755–2772 (2015).
32. Cabre, A., Marinov, I. & Gnanadesikan, A. Global atmospheric teleconnections and multidecadal climate oscillations driven by Southern Ocean convection. *J. Clim.* **30**, 8107–8126 (2017).
33. Dufour, C. O. et al. Preconditioning of the Weddell Sea polynya by the ocean mesoscale and dense water overflows. *J. Clim.* **30**, 7719–7737 (2017).
34. Reintges, A., Martin, T., Latif, M. & Park, W. Physical controls of Southern Ocean deep-convection variability in CMIP5 models and the Kiel Climate Model. *Geophys. Res. Lett.* **44**, 6951–6958 (2017).
35. Martin, T., Park, W. & Latif, M. Multi-centennial variability controlled by Southern Ocean convection in the Kiel Climate Model. *Clim. Dynam.* **40**, 2005–2022 (2013).
36. Zhang, L. & Delworth, T. L. Impact of the Antarctic bottom water formation on the Weddell Gyre and its northward propagation characteristics in GFDL model. *J. Geophys. Res. Oceans* **121**, 5825–5846 (2016).
37. Zhang, L., Delworth, T. L. & Jia, L. Diagnosis of decadal predictability of Southern Ocean sea surface temperature in the GFDL CM2.1 model. *J. Clim.* **30**, 6309–6328 (2017).
38. Lecomte, O. et al. Vertical ocean heat redistribution sustaining sea-ice concentration trends in the Ross Sea. *Nat. Commun.* **8**, 258 (2017).
39. Thompson, D. W. J. et al. Signatures of the Antarctic ozone hole in Southern Hemisphere surface climate change. *Nat. Geosci.* **4**, 741–749 (2011).
40. Cheon, W. G., Park, Y., Toggweiler, J. R. & Lee, S. The relationship of Weddell Polynya and open-ocean deep convection to the Southern Hemisphere westerlies. *J. Phys. Ocean.* **44**, 694–713 (2014).
41. Seviour, W. J. M., Gnanadesikan, A. & Waugh, D. W. The transient response of the Southern Ocean to stratospheric ozone depletion. *J. Clim.* **29**, 7383–7396 (2016).
42. Turner, J. et al. Absence of 21st century warming on Antarctic Peninsula consistent with natural variability. *Nature* **535**, 411–415 (2016).

43. Delworth, T. L. & Zeng, F. Simulated impact of altered Southern Hemisphere winds on the Atlantic Meridional Overturning Circulation. *Geophys. Res. Lett.* **35**, L20708 (2018).
44. Ferreira, D., Marshall, J., Bitz, C. M., Solomon, S. & Plumb, A. Antarctic Ocean and sea ice response to ozone depletion: a two-time-scale problem. *J. Clim.* **28**, 1206–1226 (2015).
45. Stössel, A. et al. Controlling high-latitude Southern Ocean convection in climate models. *Ocean Model.* **86**, 58–75 (2015).
46. Stuecker, M. F., Bitz, C. M. & Armour, K. C. Conditions leading to the unprecedented low Antarctic sea ice extent during the 2016 austral spring season. *Geophys. Res. Lett.* **44**, 9008–9019 (2017).
47. Zhang, L. et al. Estimating decadal predictability for the Southern Ocean using the GFDL CM2.1 model. *J. Clim.* **30**, 5187–5203 (2017).
48. Rysgaard, S. et al. Sea ice contribution to the airsea CO_2 exchange in the Arctic and Southern Oceans. *Tellus B* **63**, 823–830 (2011).
49. Brierley, A. S. et al. Antarctic krill under sea-ice: elevated abundance in a narrow band just south of ice edge. *Science* **295**, 1890–1892 (2002).
50. Leung, S., Cabre, A. & Marinov, I. A latitudinally banded phytoplankton response to 21st century climate change in the Southern Ocean across the CMIP5 model suite. *Biogeoscience* **12**, 5715–5734 (2015).
51. Rayner, N. A. et al. Global analyses of sea surface temperature, sea ice, and night marine air temperature since the late nineteenth century. *J. Geophys. Res.* **108**, 4407 (2003).
52. Smith, T. M., Reynolds, R. W., Peterson, T. C. & Lawrimore, J. Improvements to NOAAs historical merged landocean surface temperature analysis (18802006). *J. Clim.* **21**, 2283–2296 (2008).
53. Cavalieri, D. J., Parkinson, C. L., Gloersen, P. & Zwally H. J. *Sea Ice Concentrations from Nimbus-7 SMMR and DMSP SSM/I-SSMIS Passive Microwave Data, Version 1* (NASA National Snow and Ice Data Center Distributed Active Archive Center, 1996); https://doi.org/10.5067/8GQ8LZQVL0VL
54. Compo, G. P. et al. The Twentieth Century Reanalysis project. *Q. J. R. Meteorol. Soc.* **137**, 1–28 (2011).

Acknowledgements

We thank L. M. Polvani and M. Bushuk for their helpful discussions on the preliminary results. We thank L. Zanna and M. Bushuk for their valuable suggestions and comments on our paper as internal reviewers. We thank A. Shao and M. Harrison for their great help in producing closed heat budget terms in SPEAR_AM2 model.

Author contributions

L.Z. and T.L.D. conceived the idea and wrote the paper. L.Z. wrote the first draft, performed the analysis and conducted the sensitivity experiments. T.L.D. and W.C. lead the development of the SPEAR_AM2 model. X.Y. leads the SLP assimilation based on the SPEAR_AM2 model. All authors contributed to improving the manuscript.

Competing interests

The authors declare no competing interests.

Additional information

Supplementary information is available for this paper at https://doi.org/10.1038/s41558-018-0350-3.

Reprints and permissions information is available at www.nature.com/reprints.

Correspondence and requests for materials should be addressed to L.Z.

Publisher's note: Springer Nature remains neutral with regard to jurisdictional claims in published maps and institutional affiliations.

Methods

Observations. Here we use the HadISST[51] and ERSST[52] version 3 to calculate the SO area mean (50°70° S, 0°360° E) SST time series. The observed linear SST trends over 1979–2012 are based on the HadISST data. The SIE time series and SIC trends over 1979–2012 are calculated from the NSIDC[53] NASA TEAM and HadISST as well. The SIE is defined as the area where SIC is 15% or more in the SO. The SLP trend is calculated from the Twentieth Century Reanalysis version 2 (20CRv2[54]). A similar SLP trend is obtained if we use ERA-Interim reanalysis[55], albeit with smaller magnitude. Note that the annual trend patterns of SST, SIC and SLP in observations are not sensitive to the choice of ending years such as 2013, 2014 and 2015. The trends are a little lower when the end year is 2016 due to the occurrence of the Weddell Polynya at the end of 2016. We choose the year 2012 to better compare with the model historical run in which the realistic time-evolving radiative forcing ends at 2012 and we use future projection forcings thereafter. This radiative forcing is designed for CMIP5. The 20CRv2 reanalysis also ends in 2012. We use a two-sided Student *t*-test to check the significance of linear trends.

SPEAR_AM2 model. We use one model from a new set of coupled ocean–atmosphere models developed at the Geophysical Fluid Dynamics Laboratory (GFDL). The set is collectively called SPEAR (Seamless System for Prediction and Earth System Research). In this study we use an early prototype version from this set of models, called SPEAR_AM2. This model uses the same atmosphere–land model as documented in ref. [56], but at a coarser spatial resolution (atmosphere/land grid cells in SPEAR_AM2 are approximately 200 km on each side). The ocean and sea-ice components are based on the new MOM6 code, and have a horizontal resolution of approximately 1° in the subtropics, which is refined to approximately 0.5° in both latitude and longitude at high latitudes. The grid is also refined meridionally to 0.3° in the deep tropics. There are 75 layers in the vertical, with 2 m resolution near the surface. The sea-ice component in SPEAR_AM2 is called the GFDL Sea Ice Simulator (SIS2). SIS2 is a dynamical model with three vertical layers, one snow and two ice, and five ice thickness categories. The MOM6 code is available at https://github.com/NOAA-GFDL/MOM6.

A 3,300 year control simulation was conducted with atmospheric composition fixed at pre-industrial concentrations. We only present the AABW cell evolution in the first 2,000 years in the current paper. In the model, the AABW index is used to represent the strength of SO deep convection, which is defined as the absolute value of minimum global MOC (GMOC) south of 60° S in density space (Supplementary Fig. 2 in supplementary information). As mentioned in our previous paper[32,33], the AABW index correlates well with other indices related to convection such as smoothed SO SST, subsurface temperature, SIE and MLD. In contrast to surface variables, the AABW cell signal in the model is smoother due to a relative lack of high-frequency atmosphere perturbations. The peak time of convection (non-convection) is defined as the maximum (minimum) value of the AABW cell index during one cycle. The composite analysis of the internal cycle spans the time from the 1,100th year to the 1,900th year, so there are five convection cycles in total. The peak convection time in each cycle corresponds to the year when the AABW cell index has its maximum value. We also performed historical simulations with 30 ensemble members initialized from different points of the control run selected at 50 yr intervals. In these historical runs the model was forced with estimates of changing radiative forcing over the period 1860–2012, including changing greenhouse gases, changing anthropogenic and natural aerosols, solar irradiance changes and land use changes. Linear trends over 1979–2012 are calculated for SST, SIC and SLP. We only show the ensemble mean results in Fig. 1d,e, which primarily reflects the forced signal. To test the dependence of the SO transient climate response on initial conditions, we conducted three ensembles of simulations with identical historical radiative forcings but different ocean initial conditions. These three ensembles were started from points in the control simulation with differing characteristics of SO deep convection. One ensemble starts from ocean conditions in the control simulation with strong SO convection (indicated by red dots in Fig. 2a); a second ensemble starts from periods of weak SO deep convection (blue dots in Fig. 2a), while a third ensemble starts from conditions in which SO deep convection is close to a climatological mean (green dots in Fig. 2a). Since we output restart files only every 5 yr in the long control run, we use as initial conditions the restart file from the time closest to peak convection. Each ensemble has five (for peak convection cases) or six members (for the neutral convection case; even numbers guarantee the number of members moving from an inactive state to an active state is equal to the number of members moving from an active state to an inactive state), and each member starts from calendar year 1976 and integrates forward for 40 years. The linear trends over 1979–2012 are then calculated using the mean results from each ensemble. Note that the trend patterns of SST, SIC and SLP in model simulations started from active convection are not sensitive to choice of ending year such as 2013, 2014 and 2015.

SLP assimilation. The GFDL is developing a new data assimilation system to be used for decadal prediction experiments. Here, we have called it SLP assimilation. These new assimilation data apply the ensemble adjustment Kalman filter to the fully coupled climate model SPEAR_AM2, in which the atmosphere assimilates the station-based SLP data used in the 20CRv2 atmospheric SLP reanalysis. The SLP assimilation at each time step produces an increment term for the winds. Thus, the winds (U, V) in the assimilation are also broadly consistent with the observation. We have two sets of SLP assimilation runs, both of which are forced by identical radiative forcings but with different ocean initial conditions: one starts from an active convection phase in the historical simulation and the other starts from a neutral convection phase. Both runs have 36 ensemble members, start from 1970 and integrate forward to 2012. Figures shown here are based on the ensemble mean results.

Data availability

The HadISST data are available at https://www.metoffice.gov.uk/hadobs/hadisst/data; ref. [51]. The NOAA's ERSST data set is available at https://www1.ncdc.noaa.gov/pub/data/cmb/ersst/v3b; ref. [52]. The NSIDC NASA Team SIC and area data are available at http://nsidc.org/data/NSIDC-0051; ref. 53. The 20CRv2 data set is available at https://www.esrl.noaa.gov/psd/data/gridded/data.20thC_ReanV2.html; ref. [54]. The source code of ocean component MOM6 of the SPEAR_AM2 model is available at https://github.com/NOAA-GFDL/MOM6. The model experiments that support the findings of this study are available from the corresponding author on request.

References

55. Bracegirdle, T. J. et al. Assessment of surface winds over the Atlantic, Indian, and Pacific Ocean sectors of the Southern Ocean in CMIP5 models: historical bias, forcing response, and state dependence. *J. Geophys. Res.* **118**, 547–562 (2013).
56. Vecchi, G. A. et al. On the seasonal forecasting of regional tropical cyclone activity. *J. Clim.* **27**, 7994–8016 (2014).